International Journal of Heat and Technology
Vol. 39, No. 1, February, 2021, pp. 73-88
Journal homepage: http://iieta.org/journals/ijht

Numerical Prediction of Deposition in Two-Phase Flow in Vertical Pipes

Xuan Li[1], Yap Yit Fatt[1*], Afshin Goharzadeh[1], John C. Chai[2], Ming Zhang[3]

[1] Department of Mechanical Engineering, Khalifa University of Science and Technology, Abu Dhabi 127788, UAE
[2] School of Computing and Engineering, University of Huddersfield, Huddersfield HD1 3DH, UK
[3] School of Energy and Power Engineering, Nanjing University of Science and Technology, Nanjing 210094, P.R. China

Corresponding Author Email: yap.fatt@ku.ac.ae

https://doi.org/10.18280/ijht.390108

Received: 2 November 2020
Accepted: 10 February 2021

Keywords:
two-phase flow, deposition, vertical pipe

ABSTRACT

This article presents a model for particle deposition in two-phase flow in vertical pipes. There are three interacting modules in the model: Fluid Transport to predict velocity and pressure, Particle Transport to predict particle distribution and Particle Deposition to predict actual attachment of particles onto surfaces. Derivation of the governing equations is presented with the numerical solution procedure outlined. For verification, limiting cases with known solutions are considered. For validations, two-phase flows without deposition are considered. Upon verifications and validations, the model is employed to investigate particle deposition in two-phase flow with different flow patterns in both constant and variable cross section pipes, directly demonstrated the need to account for finite deposit thickness.

1. INTRODUCTION

Particles are carried in many engineering two-phase flows. These particles are prone to deposit onto surfaces of flow passages, forming a detrimental deposit layer. For examples, asphaltene, wax or hydrate deposition in oil-water or oil-gas flow in wellbores/pipelines and biological and chemical foulings in liquid-vapor flow in pipes/heat exchangers. Two-phase flow with deposition coupled involves complex interacting transport phenomena. Understanding of these interactions is required to devise effective mitigation strategy. Many experimental studies were conducted to investigate deposition in two-phase flow [1-6]. These experiment results provide an understanding of the deposition mechanism and changes in two-phase flow patterns due to the growing deposit layer. Apart from experimental studies, modeling furnishes additional understandings leading to possibly accurate prediction of deposition in two-phase flow. However, modeling becomes complex and demanding in the presence of multiple evolving interfaces, including between the two immiscible fluids and that separating the fluids from the deposit.

For deposition in two-phase flow, there are three interacting phases, i.e. two fluids and solid deposit. Such dynamic interactions between phases require three different but interacting and fully coupled modeling modules with each accounting for different transport phenomenon. These modules are Fluid Transport, Particle Transport and Particle Deposition. Fluid Transport describes the fluid flow modeled for examples using homogeneous [7-13] or separated model [14-21]. Particle Transport describes the temporally and spatially changing particle distribution either using a Lagrangian [22-25] or a Eulerian approach [26-31]. Particle Deposition predicts the actual particle attachment onto the fluid-deposit interface modeled by defining a critical length [32, 33], a critical particle velocity [34, 35], a sticking probability [36-39] or employing an m-th order deposition reaction [40, 41]. The existing literatures for modeling of deposition in two-phase flow is very limited. These limited available works will be reviewed next in the context of the above three modules.

A one-dimensional steady-state two-phase flow model for paraffin deposition in pipelines and wellbores was developed by Apte et al. [42]. Two mechanistic models are employed for Fluid Transport to identify flow pattern and then estimate pressure drop for horizontal/near-horizontal pipelines [43] and inclined/vertical wellbores [44]. For Particle Transport, molecular diffusion is responsible to transfer paraffin from bulk fluid to pipe wall. The paraffin concentration gradient is determined based on thermodynamic consideration of MSI [45]. As for Particle Deposition, diffusion-controlled deposition governed by Fick's law is assumed to predict paraffin deposit buildup rates. Experimental data is used to validate the model. However, the paraffin deposit thickness is found over-predicted.

Shagapov et al. [46] presented a model of quasi-steady oil-gas two-phase flow in a vertical well with paraffin deposition coupled to external heat transfer. The one-dimensional governing equations are derived for elemental macro control volume of the well. In this model, Fluid and Particle Transports are combined by determining the pressure (consisting of empirical frictional and gravitational components) and the temperature (heat transfer interacting with surrounding geological environment) with the mass concentration of phases along the well as a thermodynamic consequence. Particle Transport in the radial direction driven by molecular diffusion and thermophoresis is considered in determining paraffin deposit layer formation modeled as a crystallization process (Particle Deposition). Removal of the deposit layer by flow is incorporated into the model. Parametric studies performed showed that the presence of paraffin deposit increases heat losses and therefore decreases

temperature due to the increases in pressure and reduction in flow area.

Ramirez-Jaramillo et al. [47] proposed a multiphase (oil/gas/asphaltene/water) multi-component asphaltene deposition model in oil wells. The fluid is assumed as the Casson type. Generally, a framework similar to that of Ref. [46] is adopted. Using empirical correlations, both pressure and temperature are evaluated to determine thermodynamically asphaltene particle precipitation via SAFT-VR equation of state. Particle Transport in the radial direction towards the wall is accounted for by Fick's law. Particle Deposition is assumed diffusion-controlled, i.e. equaling to the amount of particles diffused to the wall. Besides deposition, deposit removal due to shear stress is included by employing the model of Kern and Seaton [48]. Therefore, the actual deposit growth is the net of deposition and removal. Interestingly, the sensitivity analysis infers constant deposit growth rate independent of the flowrate.

Huang et al. [49] proposed a two-dimensional model for wax deposition in oil-water stratified two-phase flow between two parallel plates. For Fluid Transport, the flow is assumed laminar and unidirectional. With this, the analytical expressions for velocity and pressure can be obtained from two-dimensional Navier-Stokes equations. For Particle Transport, mass balance equation with axial convection and radial diffusion is solved for the wax particle concentration. Axial diffusion and precipitation of wax particles in the oil are neglected. For Particle Deposition, wax deposit layer growth is predicted using the model of Singh et al. [50] where it is driven by radial convection in fluid and radial diffusion into the deposit. Results show that near the inlet, the wax deposit is increasingly thicker along the channel, then it becomes thinner downstream as the amount of wax decreases in oil due to deposition.

Haghshenasfard et al. [51] presented a numerical study for calcium sulphate fouling in two-phase bubbly sub-cooled boiling flow. For Fluid Transport, the multi-component two-fluid model is used to determine the velocity and pressure of various phases. For Particle Transport, the species conservation equation for each phase with convection, diffusion and source/sink accounted for is used. Finally, fouling is assumed as a surface reaction with the deposition rate given by Bohnet [52]. Results reveal an interesting decrease in the deposition rate when fluid velocity increases.

Duan et al. [53] proposed a model for wax deposition in oil-gas two-phase stratified flow in horizontal pipe. The geometry considered is three-dimensional. However, the flow is assumed fully developed and unidirectional flowing only in the axial direction. This greatly reduces the computational cost. Axial momentum with bipolar coordinate introduced to facilitate representing the oil-gas interface is solved subjected to satisfying both the given oil and gas mass flowrates. Wax particle is transported by convection and diffusion. For Particle Deposition, it is assumed to be diffusion-controlled, i.e. the deposition flux depends entirely on the wax particle concentration gradient at the wall.

Alhosani et al. [54] presented a one-dimensional model for asphaltene deposition in oil-gas flow in wellbore. For a given flow condition, the flow pattern (categorized as either bubble, slug, churn, dispersed bubble or annular flow) is first determined. Then, the pressure drop is determined by employing various empirical correlations specific for the flow pattern. For Particle Transport, asphaltene particle is to be only driven by convection along the wellbore. Particle deposition is assumed driven by radial particle concentration gradient characterized in the form of a transport coefficient and a sticking probability. The deposit thickness is then calculated.

In the above works, the deposit layer evolving over time is usually assumed having no effect on flow fields. For example, the deposit layers dealt with in Ref. [49, 51] were assumed thin, in view of the modeling complication of a moving boundary problem. The deposit layers were treated as a thermal insulation layer which only altered the overall heat transfer coefficient between the fluid and the pipe wall, no effect on the flow field is considered [42, 47]. Although pressure drop was correlated to the thickness of paraffin deposits, velocity fields were considered stationary during the operation of a well, i.e. not affected by the presence of a growing deposit layer [46]. Only in the work of [54] is the effect of deposit thickness considered to affect the two-phase fluid flow. Particle Deposition results in the evolution of a deposit layer. The growing evolving deposit layer does reduce flow area, leading to the changes in both velocity and pressure fields, i.e. affecting the fluid flow (Fluid Transport). This in turn changes the particle distribution (driven by convection and diffusion), i.e. Particle Transport, and eventually modifies the deposition process itself. Therefore, these processes are actually fully-coupled. The importance of fully-coupling these processes is highlighted in by Huang at al. [49]. To the best knowledge of the authors, the fully-coupled nature has not been addressed conclusively in the existing works as so far. In this regard, this study presents a general approach to model deposition in two-phase flow with Fluid Transport, Particle Transport and Particle Deposition fully-coupled.

The remainder of the article is divided into six sections. The problem description is first presented in Section 2. The mathematical formulation is given in Section 3. The solution procedure is then outlined in Section 4. In Section 5, the model is verified, validated and employed to investigate particle deposition in various pipes. Finally, the present article concludes with a few remarks in Section 6.

2. PROBLEM DESCRIPTION

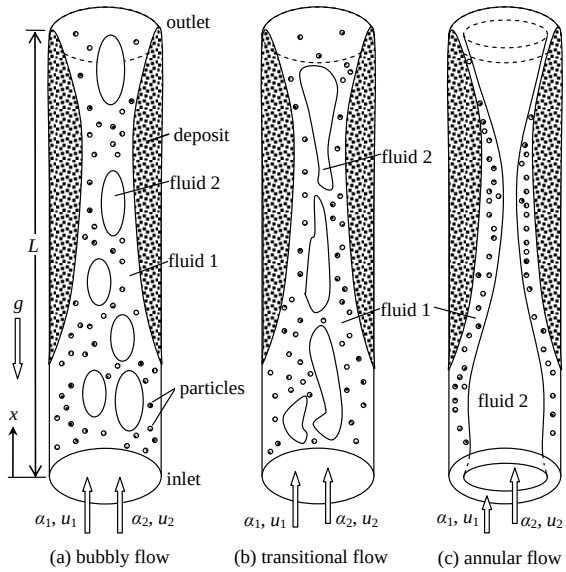

Figure 1. Deposition in a two-phase flow in a vertical pipe

Figure 1 shows three circular vertical pipes with each containing three phases, i.e. two immiscible fluids (fluid 1 and

fluid 2) and solid particles. The corresponding two-phase flow patterns are bubbly, transitional and annular. The particles are carried by fluid 1 only. These particles deposit gradually onto the wall forming a deposit layer attached to the pipe wall. Over time, the deposit layer becomes thicker and reduces the flow area. The fluid velocity and pressure fields then vary correspondingly, potentially changing the two-phase flow pattern. During deposition, particles are consumed, i.e. converted into deposit, the particle concentration in fluid 1 decreases.

3. MATHEMATICAL FORMULATION

The following assumptions are made:

(a) One-dimensional flow.

In many engineering applications, the ratio of pipe length to diameter L/d is exceedingly large. Pipes with length of tens of meters but diameter of a few centimeters are commonly encountered, i.e. L/d is in the order of 10^2. In the oil and gas industry, for a wellbore of length in terms of km but diameter in terms of cm, L/d easily reaches a ratio in the order of 10^5 [55]. For two-phase flow with the additional physics of particle deposition (with interface tracking/capturing for the fluid-fluid interface and fluid-deposit front), a fully three-dimensional or even an axisymmetric model is computation very expansive. Hence, it is not sought here. In the current article, we propose to employ a one-dimensional model for these types of problems with a more practically affordable numerical solution and yet provide sufficient realistic solution in guiding operational decision to be made.

(b) Common pressure for the two fluids.

In two-phase separate flow model [56, 57], the pressure is assumed common for the two fluids. As this model is used here in this study, the same assumption is made.

(c) Dilute particle concentration, i.e. particles do not interact with each other.

For many engineering applications, the concentration of depositing particle is very low. For example, asphaltene deposition issues in wellbore/pipelines plaguing the oil and gas industries, the flowing oil has an asphaltnene particle concentration in the order of less than 1% volume fraction [41, 58, 59]. Although the volume fraction is small, the deposit forms over time can substantially block the flow area of wellbore/pipelines.

(d) Rigid and immobile deposit.

Deposit once formed, generally attached well to surfaces and often ages (becomes compacted and hardened, i.e. more rigid) over time. Of course, the deposit can no longer flow. Hence, in the current model, the deposit assumes rigid and immobile.

(e) Negligible particle diffusion along the pipe (compared to convection).

For problems of interest here with a large L/d, the Peclet number is large, i.e. diffusion transport of particles along the pipe is much smaller than convection transport along the pipe. Therefore, it is assumed to have negligible diffusion transport of particles.

There are three modules with each describing different physics of the model: Fluid Transport for prediction of velocity and pressure, Particle Transport for prediction of particle distribution and Particle Deposition for modeling the actual particle attachment onto the wall. These modules are presented next.

3.1 Fluid transport

For the particles, fluid 1 and fluid 2, the mass conservation equations are given respectively as:

$$\frac{\partial}{\partial t}(\rho_d \alpha_d) = \dot{M}_d \alpha_1 \tag{1}$$

$$\frac{\partial}{\partial t}(\rho_1 \alpha_1) + \frac{\partial}{\partial x}(\rho_1 u_1 \alpha_1) = -\dot{M}_d \alpha_1 \tag{2}$$

$$\frac{\partial}{\partial t}(\rho_2 \alpha_2) + \frac{\partial}{\partial x}(\rho_2 u_2 \alpha_2) = 0 \tag{3}$$

where, α, ρ and u are respectively volume fraction, density and velocity. The subscripts d, 1 and 2 represent respectively quantities associated with deposit, fluid 1 and fluid 2. Note that α_d, α_1 and α_2 satisfy

$$\alpha_d + \alpha_1 + \alpha_2 = 1 \tag{4}$$

where, $\dot{M}_d$ is the volumetric particle deposition rate representing the amount of particles attached (deposited) onto the fluid-deposit interface. Eqns. (1), (2) and (3) can be combined into:

$$\begin{aligned}\frac{\partial}{\partial t}(\rho_d \alpha_d) + \frac{\partial}{\partial t}(\rho_1 \alpha_1) + \frac{\partial}{\partial t}(\rho_2 \alpha_2) \\ + \frac{\partial}{\partial x}(\rho_1 u_1 \alpha_1) + \frac{\partial}{\partial x}(\rho_2 u_2 \alpha_2) = 0\end{aligned} \tag{5}$$

For fluid 1 and fluid 2, the momentum conservation equations can be respectively expressed mathematically as:

$$\begin{aligned}\frac{\partial}{\partial t}(\alpha_1 \rho_1 u_1) + \frac{\partial}{\partial x}(\alpha_1 \rho_1 u_1^2) \\ = -\alpha_1 \frac{\partial p}{\partial x} - F_{w1} + F_{12} - \alpha_1 \rho_1 g - \alpha_1 \dot{M}_d u_1\end{aligned} \tag{6}$$

$$\begin{aligned}\frac{\partial}{\partial t}(\alpha_2 \rho_2 u_2) + \frac{\partial}{\partial x}(\alpha_2 \rho_2 u_2^2) \\ = -\alpha_2 \frac{\partial p}{\partial x} - F_{w2} - F_{12} - \alpha_2 \rho_2 g\end{aligned} \tag{7}$$

where, p and g are respectively pressure and gravitational acceleration. The interfacial forces: F_{w1}, F_{w2} and F_{12} are respectively between the wall and fluid 1, the wall and fluid 2 and between two fluids. Interfacial forces depend on flow patterns. The flow is demarcated into three flow patterns: bubbly, transitional and annular flow. These interfacial forces, calculated using the approaches of [57, 60, 61], are presented in the Appendix.

3.2 Particle transport

Driven by flow and in the presence of deposition, the particle distribution in the pipe changes with time. The particle concentration C in the pipe is governed by species conservation equation as:

$$\frac{\partial}{\partial t}(\alpha_1 C)+\frac{\partial}{\partial x}(\alpha_1 u_1 C)=-\dot{M}_d\alpha_1 \tag{8}$$

3.3 Particle deposition

Particle deposition is the actual attachment of particles onto solid surface. By assuming an m-th order deposition reaction [41], the deposition rate can be determined as:

$$\dot{M}_d = kC^m \tag{9}$$

with k as the deposition rate constant. The deposition reaction order is currently set to m=1. Higher order deposition reaction order can be employed as well.

4. SOLUTION PROCEDURE

Eqns. (1), (2), (3), (6), (7) and (8) are reformulated in a general transient-convection equation, expressed as:

$$\frac{\partial}{\partial t}(\tilde{\rho}\varphi)+\frac{\partial}{\partial x}(\tilde{\rho}u\varphi)=S_\varphi \tag{10}$$

where, ϕ is the variable of interest, i.e. α_d (Eq. 1), α_1 (Eq. 2), α_2 (Eq. 3), u_1 (Eq. 6), u_2 (Eq. 7) and C (Eq. 8). In Eq. (10), $\tilde{\rho}$, u and S_φ are respectively the appropriate 'density', appropriate velocity and source term.

A finite volume method [62] is employed to solve this general transient-convection equation. As illustrated in Figure 2, the pipe is discretized into N non-overlapping control volumes (CVs). The P-CV (hatched) spans from the CV surface at W to P. Both scalar (α_d, α_1, α_2, p and C) and vectorial (u_1 and u_2) variables are stored at the surface of the CVs, e.g. at W, P, E, etc. Eq. (9) is integrated over the P-CV using a fully implicit time integration scheme as:

$$\frac{\partial}{\partial t}\int_{\Delta V}\tilde{\rho}\varphi dV+\int_{\Delta V}\frac{\partial}{\partial x}(\tilde{\rho}\bar{u}\varphi)dV=\int_{\Delta V}S_\varphi dV \tag{11}$$

$$\frac{(\tilde{\rho}\varphi)_P^{n+1}-(\tilde{\rho}\varphi)_P^{n}}{\Delta t}\Delta V + (\tilde{\rho}u\varphi A)_P^{n+1}-(\tilde{\rho}u\varphi A)_W^{n+1}=(S_\varphi)_P^{n+1}\Delta V \tag{12}$$

The value at P is assumed to prevail over the P-CV. The superscript n and n+1 refers to quantities associated with time t and $t+\Delta t$. Dropping these indices for time, and instead employ the superscript o for quantities associated with time t, upon rearrangement, Eq. (12) becomes:

$$a_P\varphi_P=a_W\varphi_W+b \tag{13a}$$

$$a_P=(\tilde{\rho}uA)_P+\frac{\tilde{\rho}_P\Delta V}{\Delta t} \tag{13b}$$

$$a_W=(\tilde{\rho}uA)_W \tag{13c}$$

$$b=\frac{\tilde{\rho}_P^o\varphi_P^o\Delta V}{\Delta t}+(S_\varphi)_P\Delta V \tag{13d}$$

Note that the variables need to be solved, i.e. φ_P at node P at time $t+\triangle t$, are only related to *known* values at node P at time t (φ_P^o) and at the upstream node W at time $t+\triangle t$ (φ_W). Therefore, using a marching procedure in the direction of time and from upstream to downstream, the solutions at time $t+\triangle t$ can then be easily obtained. To couple the velocities and pressure, two-phase SIMPLER algorithm [63] with reformation to consider the changing flow area due to deposition is employed. The overall solution algorithm is summarized below. For detailed solution procedure, please refer to [64].

(1) Specify the inlet values at i=1 and the initial conditions at t=0.
(2) Advance time step from t to $t+\Delta t$.
(3) Solve Eqns. (5) to (7) for u_1, u_2 and p using two-phase SIMPLER algorithm [63].
(4) Solve Eq. (1) for α_d.
(5) Solve Eq. (2) for α_1.
(6) Solve Eq. (4) for α_2.
(7) Solve Eq. (8) for C.
(8) Iterate steps (3) to (7) until the solution converges.
(9) Iterate steps (2) to (8) for all subsequent time steps.

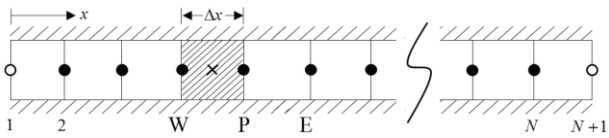

Figure 2. Discretized computational domain

5. RESULTS AND DISCUSSIONS

5.1 Verification: Single-phase "bubbly" flow with deposition

A *single-phase* "bubbly" flow in a vertical pipe of L=10m is first considered for verification purpose. The continuous fluid 1 contains particles. There is no particle in the dispersed fluid 2, i.e. bubbles. Initially, there is not deposit in the pipe. The following initial conditions apply along the entire pipe, i.e. $0\le x\le L$.

$$\alpha_d=0,\ \alpha_1=0.8,\ \alpha_2=0.2,\ u_1=u_2=0.2\ \text{m/s} \tag{14}$$

The inlet conditions remain constant as time progresses. The particles in the dispersed fluid 1 deposit on the wall with a hypothetical prescribed deposition rate of

$$\dot{M}_d=100x/L \tag{15}$$

The properties of both fluids are identical, i.e. $\rho_1=\rho_2=820$kg/m^3, $\mu_1=\mu_2=3.95\times10^{-3}$Pa·s and ρ_d=820kg/m^3. As there is actually one fluid physically present, no interfacial force between fluids acts, i.e. F_{12}=0. As such, this special "bubbly" flow is actually a single-phase flow with deposition with the following analytical solution:

$$\alpha(x,t)=1-\frac{1}{82}xt \tag{16a}$$

$$u(x,t)=\frac{1}{5\alpha} \tag{16b}$$

$$p(x,t)=\frac{16.4x(xt^2+316xt-164t-25912)}{(xt-82)^2} \tag{16c}$$

where, α is the fluid volume fraction and u is the fluid mean velocity, respectively defined as:

$$\alpha=\alpha_1+\alpha_2 \tag{16d}$$

$$u=\frac{\alpha_1 u_1+\alpha_2 u_2}{\alpha_1+\alpha_2} \tag{16e}$$

This analytical solution can be used to verify the implemented model. By setting F_{12}=0, the current model reduces to the limiting case of a single-phase flow with deposition. Figure 3 shows the mesh independent solution from a mesh of 50CVs with $\Delta t=1.0\times10^{-3}$ s. The prediction is compared to that of the analytical solution (Eq. 16). Good agreement is attained, verifying the implemented model partially (as some features of the model are switched off in this computation).

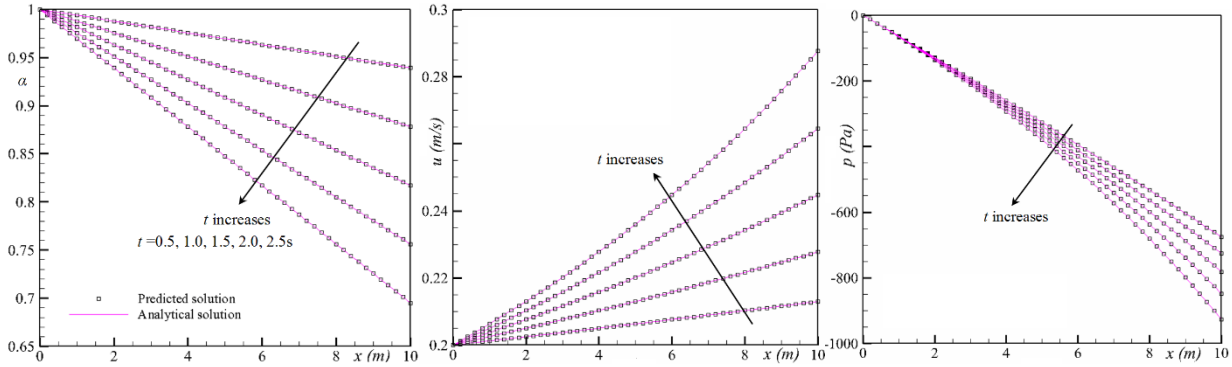

(a) fluid volume fraction (b) velocity (c) pressure

Figure 3. Prediction for single-phase "bubbly" flow with deposition

5.2 Validation: Two-phase water-kerosene bubbly flow

In this section, two-phase water-kerosene flows are investigated to validate the developed model by comparing the predictions against the available experimental data of Suguimoto and Mazza [65]. Herein, two different cases are considered: (1) kerosene drops dispersed in water (i.e. bubbly flow), and (2) water drops dispersed in kerosene (i.e. elongated drops flow). The water density and viscosity are respectively 998 kg/m^3 and 1 mPa·s. For kerosene, the density and viscosity are respectively 793kg/m^3 and 1.1 mPa·s. Surface tension between water and kerosene is 48mN/m. There is no particle in the flow (C=0) and hence no particle deposition occurs ($\dot{M}_d$=0). The numerical mesh-independent solutions of frictional pressure drop for the two cases are plotted respectively in Figures (4a) and (4b) for various water-kerosene input ratio (J_1/J_2), with experimental data superimposed. The predictions by the model are in good agreement with experimental data, validating the current model for two-phase flow prediction.

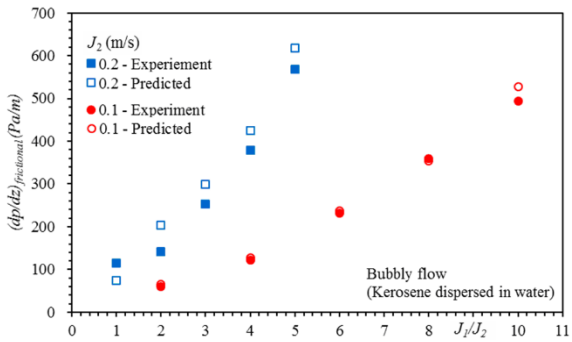

(a) kerosene drops dispersed in water

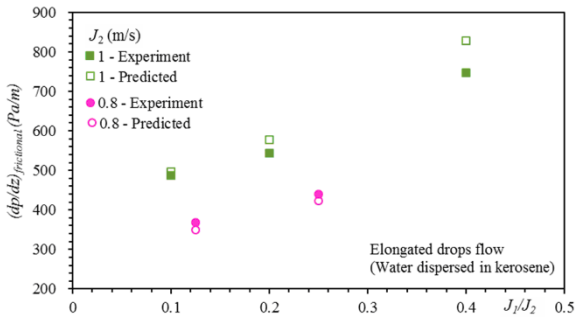

(b) water drops dispersed in kerosene

Figure 4. Frictional pressure drop for two-phase bubbly flow

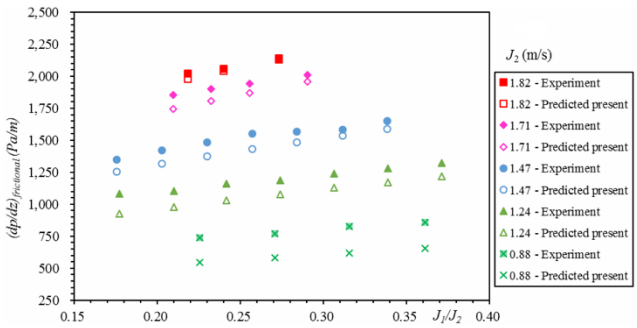

Figure 5. Frictional pressure drop for two-phase annular flow

5.3 Validation: Two-phase water-crude oil annular flow

The present model is further validated for a two-phase flow a different flow pattern. The prediction for a water-crude oil annular flow from the current model is compared against the experimental data measured of Rodriguez et al. [66]. The water density and viscosity are respectively 997 kg/m^3 and

0.89 mPa·s. For kerosene, the density and viscosity are respectively 925kg/m^3 and 500 mPa·s. Surface tension between water and kerosene is 26.3mN/m. Note that slightly different water properties are used in this validation exercise in order to be consistent with the experimental data. For the limiting case of two-phase flow without deposition, $\dot{M}_d$ =0 and C=0 are set in the present model. The mesh-independent solutions for the frictional pressure drop are shown in Figure 5. Generally, the trend for the pressure drop is captured. The predicted pressure drop agrees increasingly well with the experimental data for higher oil superficial velocity. It is noted that the uncertainties in the experimental measurement for the pressure drop are approximately ±25% under the minimum oil superficial velocity and ±6% under the maximum oil superficial velocity. This exercise validates the model for prediction of two-phase annular flow.

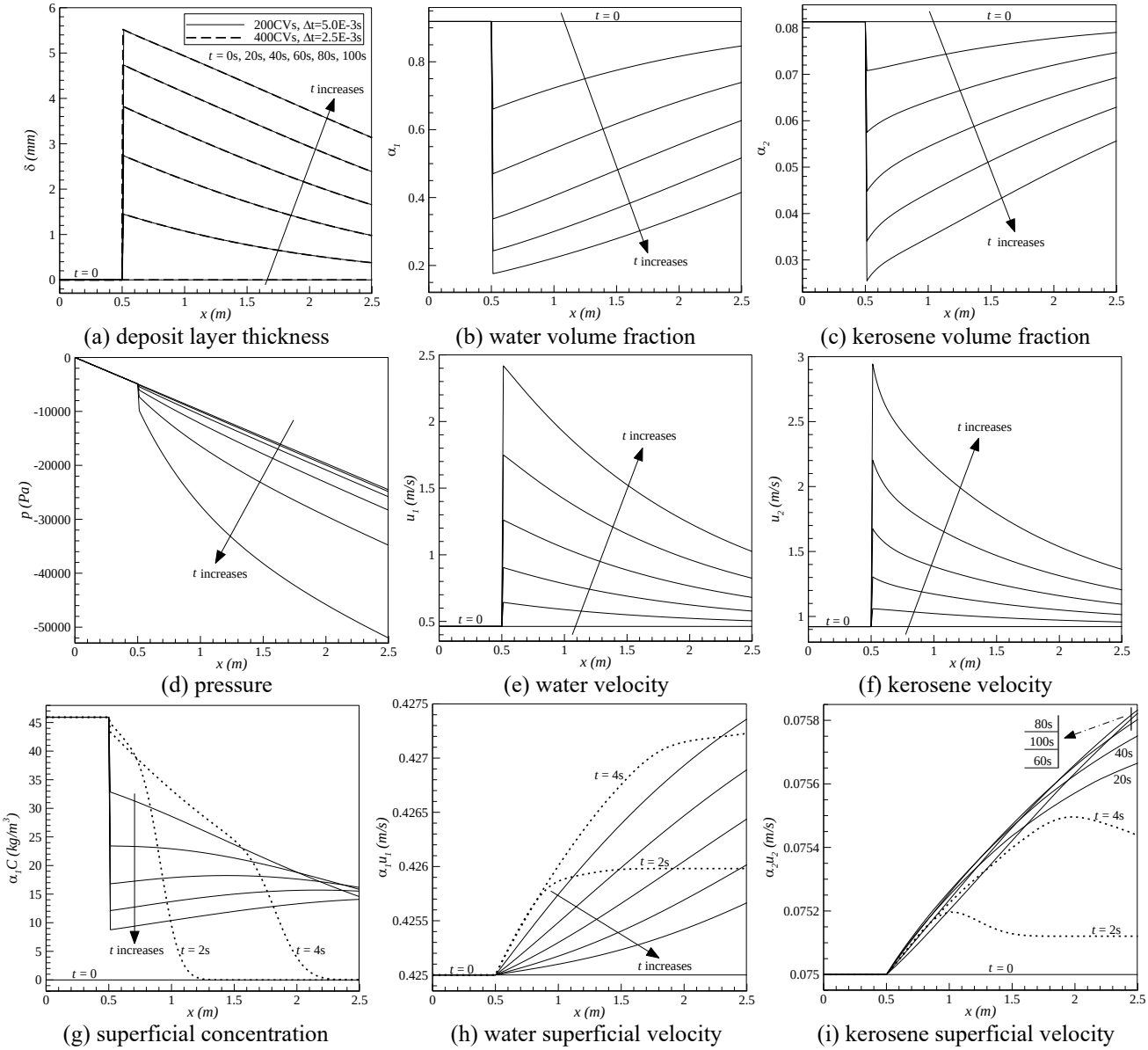

Figure 6. Bubbly flow with deposition

5.4 Deposition in two-phase flow in pipe of constant cross section

Deposition in two-phase flow in pipe of constant cross section is now investigated. Three different two-phase flows are considered: bubbly, transitional and annular flow. Figure 1a presents a two-phase bubbly flow with water as the continuous fluid 1 along with kerosene as the dispersed fluid 2 in a vertical pipe of inner diameter 0.02m and a length of 2.5m. Initially, the pipe is clean (α_d=0) with steady-state fully-developed bubbly flow of α_1=0.9186, α_2=0.0814, u_1=0.4626m/s and u_2=0.9218m/s (correspond to superficial velocities of $\alpha_1 u_1$=0.425m/s and $\alpha_2 u_2$=0.075m/s, and $\alpha_1 u_1+\alpha_2 u_2=0.50$m/s). These initial conditions are consistent with the governing equations of Eqns. (1) to (9). At time t=0$^+$, water carries particles into the pipe at the inlet with a concentration of C=50kg/m^3 (corresponds to superficial concentration of $\alpha_1 C$=45.93kg/m^3). The pipe section of x≤05m is treated with anti-deposition coating, i.e. particles do not deposit in this section. The particles deposit on the pipe wall for x>0.5m forming a deposit layer. With this, the particle deposition rate constant k is set to:

$$k = \begin{cases} 0 & , x \le 0.5 \\ 0.3\text{s}^{-1} & , x > 0.5 \end{cases} \qquad (17)$$

Figure 6 shows the results at $t = 0$, 20, 40, 60, 80, and 100s. In Figure 6, the time t=0, 20, 40, 60, 80 and 100s is stated in the first plot (Figure 6a). For all plots of Figure 6, the curve for t=0 is labeled and curves for increasing time t are given in the direction of the arrow. This approach of plotting will be employed for all remaining figures to avoid overcrowding the figures with labels. Plotted in Figure 6a is the deposit thickness along the pipe. Solution from a mesh of 200CVs with $\Delta t = 5 \times 10^{-3}$ s is considered mesh independent. There is no deposit for x<0.5m due to Eq. (17). Deposit only forms downstream.

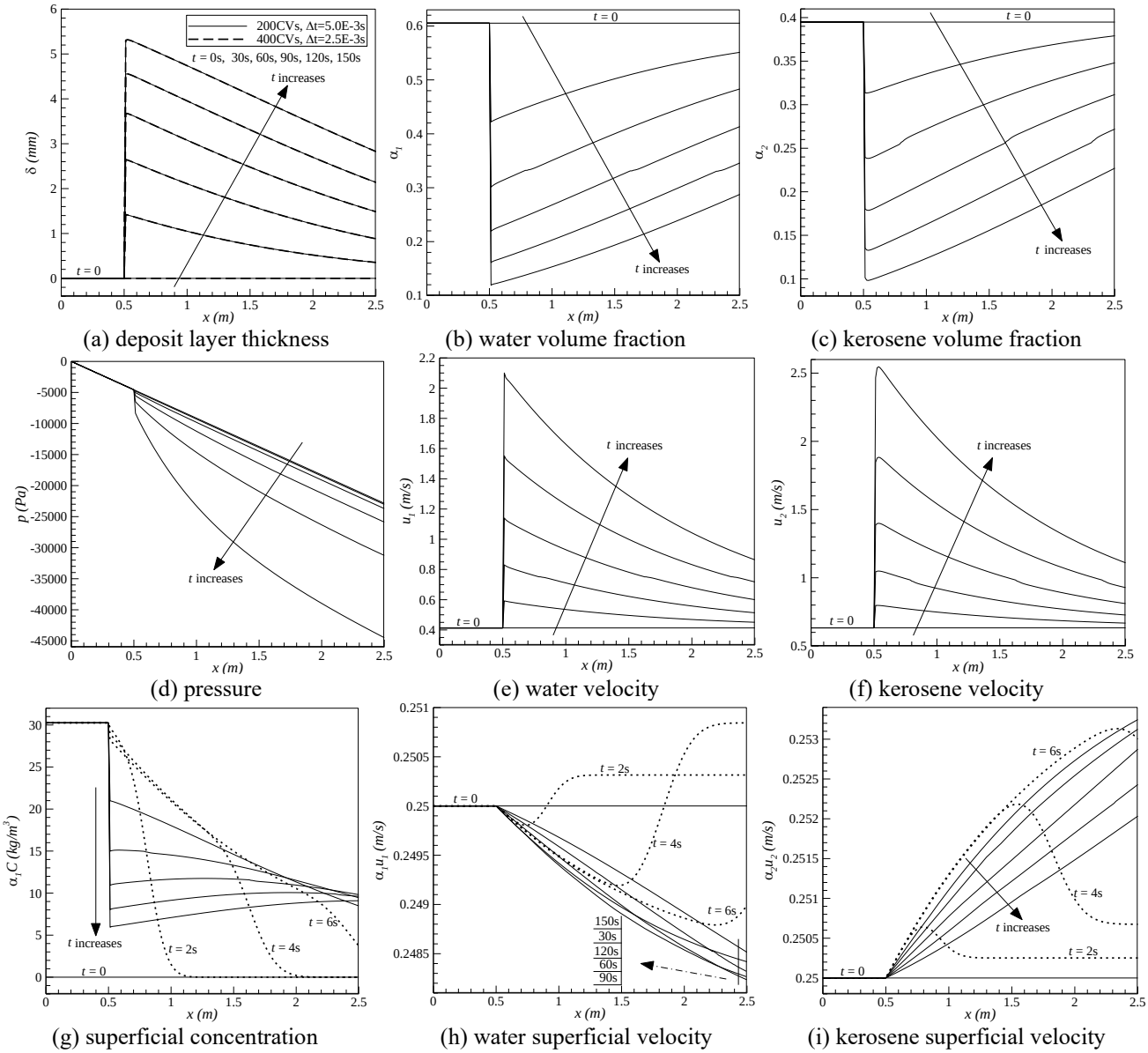

Figure 7. Transitional flow with deposition

Eqns. (8) and (9) infer that the actual amount of deposit formation rate is proportional to $\alpha_1 C$, i.e. the superficial particle concentration plotted in Figure 6g. Note that additional plots at t=2 and 4s are included as dashed lines. Deposition occurs only after t=1.08s when particles carried by water actually reach x=0.5m. For t at least up to 40s, the superficial particle concentration is highest at x=0.5m, i.e. inducing the highest particle deposition rate and therefore forming the thickest deposit layer. With particles continuously consumed in the deposition process, there are less particles flowing downstream. As a result, the superficial particle concentration reduces along the pipe and so does the particle deposition rate. Therefore, the deposit layer is thinner along the pipe. In addition, over time, the deposit layer grows and the pressure drop along the pipe increases (Figure 6d). After t>40s, particle concentration downstream can be higher than that of the upstream as the amount of particles replenished by those from the upstream is more than that deposited.

As deposit forms, the deposit volume fraction increases along the pipe and over time (reflected by δ in Figure 6a). As constrained by Eq. (4), both water and kerosene volume fractions decrease (Figure 6b and 6c). Accordingly, the available flow area (α_1+α_2) decreases. Thus, along the pipe, a sharp increase appears in the water and kerosene velocities immediately downstream of x>0.5m and followed by a gradual decrease downstream where the deposit layer becomes thinner (Figure 6e and 6f).

The actual flowrate is more appropriately reflected by the superficial velocity (Figure 6h and 6i). Near the inlet where there is no deposit, the superficial velocity for both water and kerosene remains constant. Deposit formation affects minutely the superficial velocity over time and along the pipe.

For transitional flow, with the same pipe configuration, the initial conditions are now set to steady-state fully-developed flow with α_1=0.6052, α_2=0.3948, u_1=0.4131m/s and u_2=0.6332m/s (correspond to superficial velocities of $\alpha_1 u_1$=0.25m/s and $\alpha_2 u_2$=0.25m/s, note that $\alpha_1 u_1 + \alpha_2 u_2 = 0.50$ m/s, i.e. the total volumetric flowrate is maintained). The particle concentration at the inlet is maintained as C=50kg/m^3 but the superficial concentration becomes α_1C=30.26kg/m^3.

The mesh independent solutions obtained using 200CVs with $\Delta t = 5 \times 10^{-3}$ s are plotted in Figure 7. The deposit profile is similar to that of bubbly flow, and thus so are the general trends of α_1, α_2, u_1, u_2, p and C. The deposit is thickest at x=0.5m, i.e. the same location as that of bubbly flow, then progressively thinner downstream. However, at a given time, it is thinner than that of bubbly flow (see Figures 6a and 7a for example at t=60s) as the amount of particles injected at the inlet is now smaller (given a smaller water volume fraction α_1) and therefore the deposit grows slower. With a thinner deposit layer formed at a given time, the pressure drop is of course smaller (see comparison between Figures 6d and 7d).

The initial conditions are now varied such that the flow now is of an annular nature (Figure 1c) with fluid 2 (kerosene) flowing in the core and a fluid 1 (water) layer flowing attached to the wall. Initially, the pipe is clean (α_d=0) with steady-state fully-developed annular flow of α_1=0.1819, α_2=0.8181, u_1=0.2748m/s and u_2=0.55m/s (correspond to superficial velocities of $\alpha_1 u_1$=0.05m/s and $\alpha_2 u_2$=0.45m/s, again the total volumetric flowrate is maintained). The particle concentration at the inlet is maintained as C=50kg/m^3 but the superficial concentration becomes α_1C=9.095kg/m^3.

With even smaller amount of particles injected at the inlet (Figure 8g) compared to that of bubbly flow (Figure 6g), the deposit layer now grows even much slower (Figure 8a).

It requires a much longer time to achieve a deposit layer of similar thickness. For example, to attain a maximum deposit thickness of around $\delta \approx 5$ mm (at x=0.5m), it requires 80s for bubbly flow (Figure 6a) and 500s for annular flow (Figure 8a). With this deposit layer thickness, the pressure drop incurred in annular flow (Figure 8d) is lower than that of bubbly flow (Figure 6d). For annular flow, there is not direct interaction between the more viscous kerosene and the deposit surface. Only the less viscous water is in contact with the deposit surface giving a smaller frictional pressure drop. Besides, there are more less dense kerosene than the denser water in the pipe in annular flow, resulting in a smaller gravitational pressure drop. Both of these lead to a smaller total pressure drop.

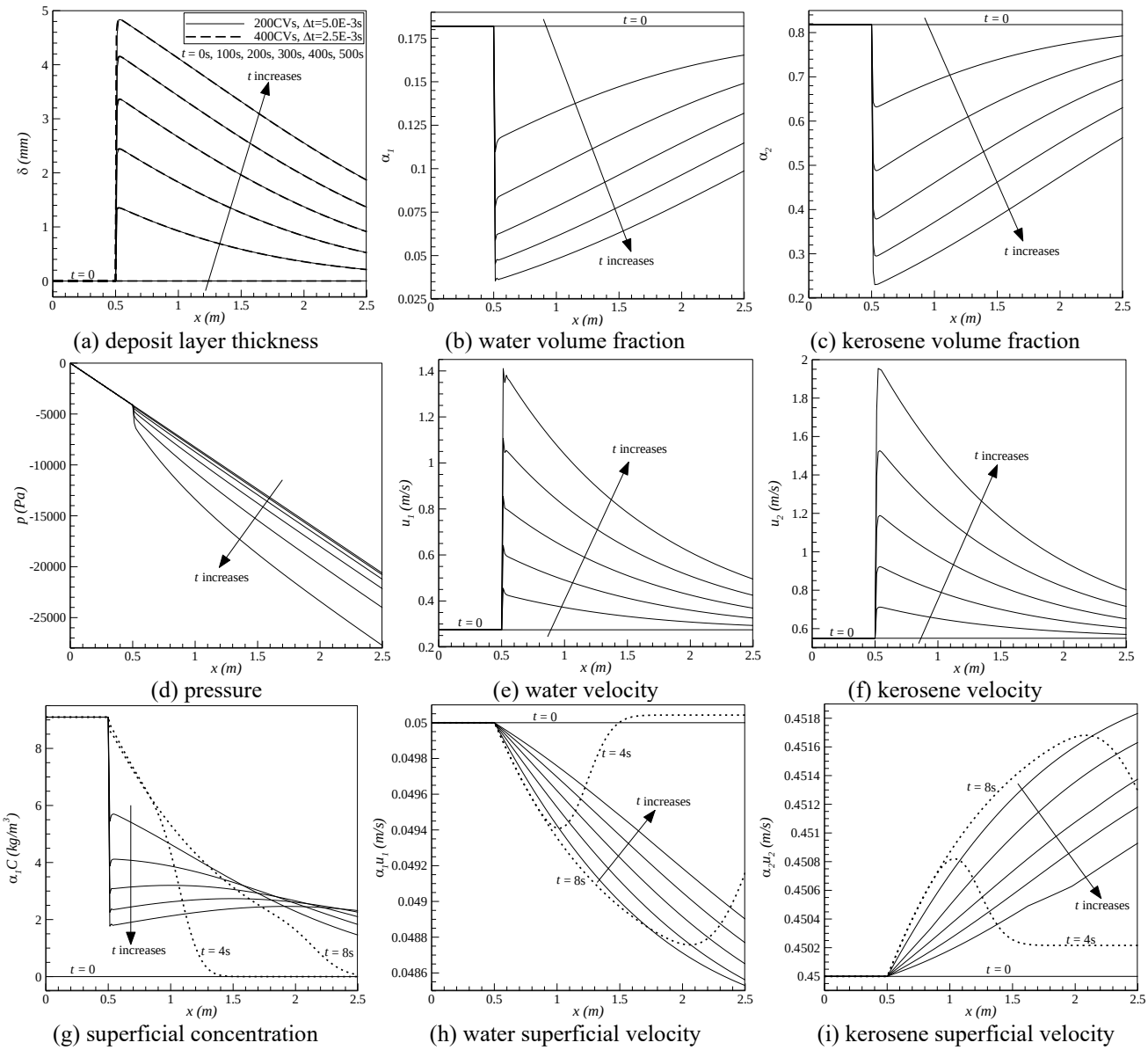

(a) deposit layer thickness (b) water volume fraction (c) kerosene volume fraction

(d) pressure (e) water velocity (f) kerosene velocity

(g) superficial concentration (h) water superficial velocity (i) kerosene superficial velocity

Figure 8. Annular flow with deposition

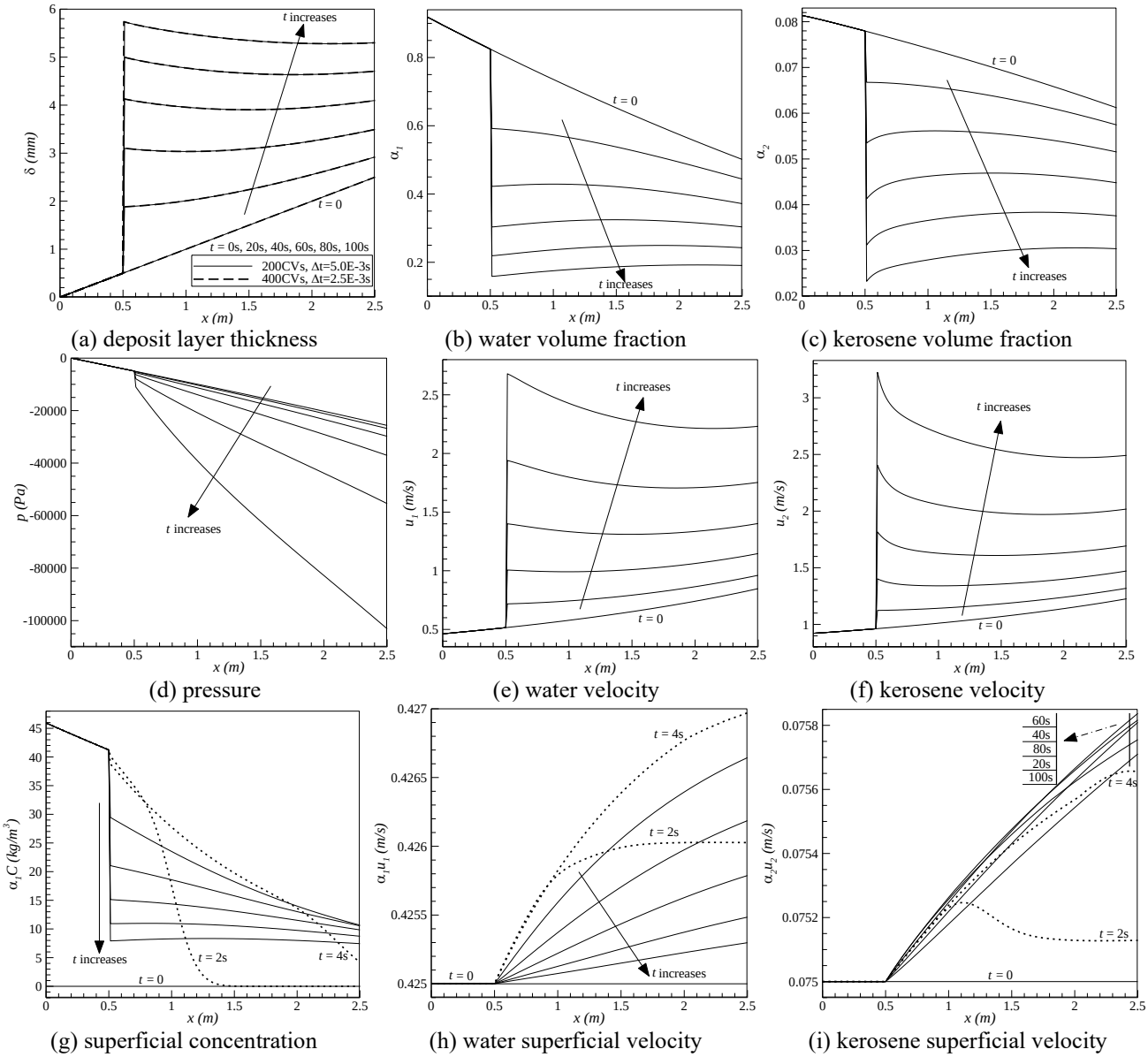

Figure 9. Deposition in a converging pipe

5.5 Deposition in two-phase flow in pipes of varying cross section

In this section, the model is applied for deposition in two-phase flow in pipes of varying cross section. The first scenario considered is a converging pipe with diameter varies linearly along the pipe according to:

$$D(x) = D_{\max} - (D_{\max} - D_{\min})\frac{x}{L} \tag{18}$$

where, the maximum and minimum diameters are respectively set to D_{max}=20×10^{-3}m and D_{min}=15×10^{-3}m. This pipe geometry is conveniently achieved in the present model by assuming that the pipe has already have a pseudo "initial deposit layer" varying along the pipe formed as:

$$\alpha_d(x) = 1 - \frac{D^2}{D_{\max}^2} \tag{19}$$

The steady-state solution for the pipe with pseudo "initial deposit layer" of Eq. (19) (with emphasis that the deposit is not growing by temporarily setting k=0 for $0 \le x \le L$, i.e. physically, the pipe is "clean") with the inlet conditions of the above bubbly flow enforced (α_1=0.9186, α_2=0.0814, u_1=0.4626m/s and u_2=0.9218m/s) is first obtained, i.e. plots for t=0s in Figure 9. The pseudo "initial deposit layer" mimicking the desired converging pipe geometry is obvious in Figure 9a. Because of the converging nature of the pipe, this steady-state solution has both water and kerosene velocities increase along the pipe, but with both volume fractions of water and kerosene decrease along the pipe for continuity to be maintained, i.e. constant flowrate for water and kerosene at a given axial location. This steady-state solution is then used as the initial condition for the actual study of deposition in two-phase bubbly flow in a converging pipe.

Plotted in Figure 9 is the mesh independent solution. Note that the actual deposit thickness formed is given by $\delta - \delta|_{t=0}$. The deposit thickness *growth* over time is very similar to that of a bubbly flow in pipe of constant cross section (comparison with Figure 6a), e.g. similar deposit thickness formed from 80s to 100s along the pipe for the two scenarios. Do note that because of the circularity of the pipe cross section, a larger amount of deposit is actually formed for the scenario of pipe of constant cross section, even though the actual deposit

thickness at a given axial location is comparable. For the converging pipe, because the flow area is now smaller ($\alpha_1 + \alpha_2$), the pressure drop incurred becomes significantly larger initially and for all time (Figures 6d and 9d). For the converging pipe, as the deposit grows over time, α_d becomes increasing constant downstream of x=0.5m (flattening of δ downstream in Figure 9a) because of the pseudo "initial deposit layer". As a result, the flow area becomes more constant downstream of x=0.5m, incurring a particularly constant pressure gradient at t=100s in stark contrast to that in pipes of constant cross section where pressure gradient decreases gradually downstream of x=0.5m (Figure 6d).

The superficial particle concentration upstream of x=0.5m is interesting. For a pipe of constant cross section, it is constant both spatially and temporally (Figure 6g). However, for a converging pipe, although remains temporally unchanged, decreases spatially along the pipe prior to x=0.5m (Figure 9g). This is because in the converging pipe, water flows faster downstream and therefore can transport the same amount of particles with a lower superficial concentration. In the early stage of deposition, the superficial concentration decreases along the pipe. With more particles available upstream, the deposit growth is faster upstream and therefore consuming more particles. Over time, the superficial concentration then decreases faster upstream. Eventually, the superficial concentration becomes almost constant along the pipe downstream of x=0.5m, e.g. at 80s and 100s.

Sinusoidal pipes are now considered. The pipe diameter varies sinusoidally along the pipe as:

$$D(x) = \frac{D_{\max} + D_{\min}}{2} + \left(\frac{D_{\max} - D_{\min}}{2}\right)\cos\left(\frac{2\pi x}{l}\right) \qquad (20)$$

where, for the second scenario: l=L (Figure 10a) and third scenario: l=$L/4$ (Figure 11a). Again the inlet conditions of the above bubbly flow (α_1=0.9186, α_2=0.0814, u_1=0.4626m/s and u_2=0.9218m/s) are enforced. The initial conditions for these scenarios are obtained using the same approach as in the above scenario of a converging pipe.

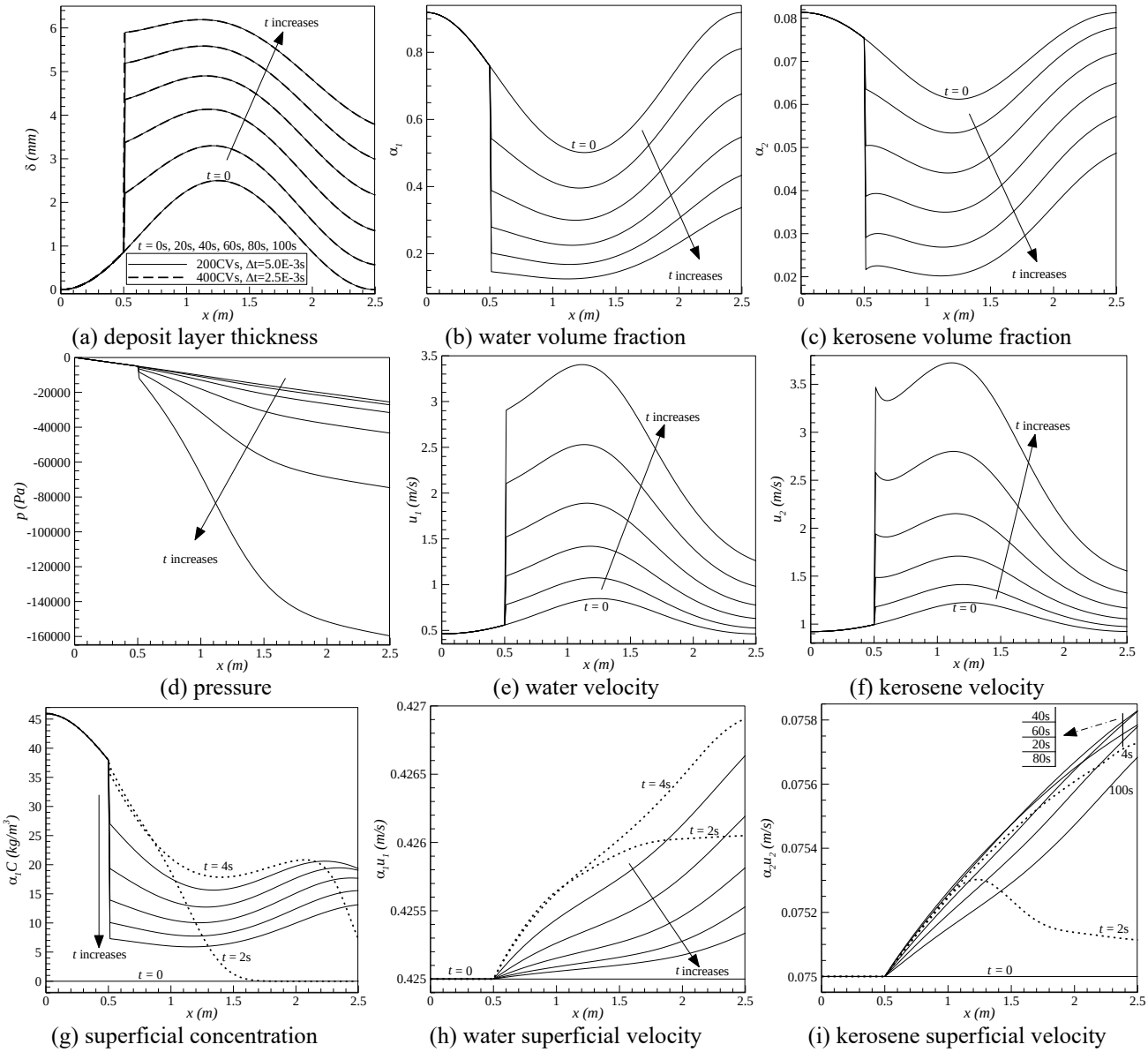

Figure 10. Deposition in a sinusoidal pipe with l=L

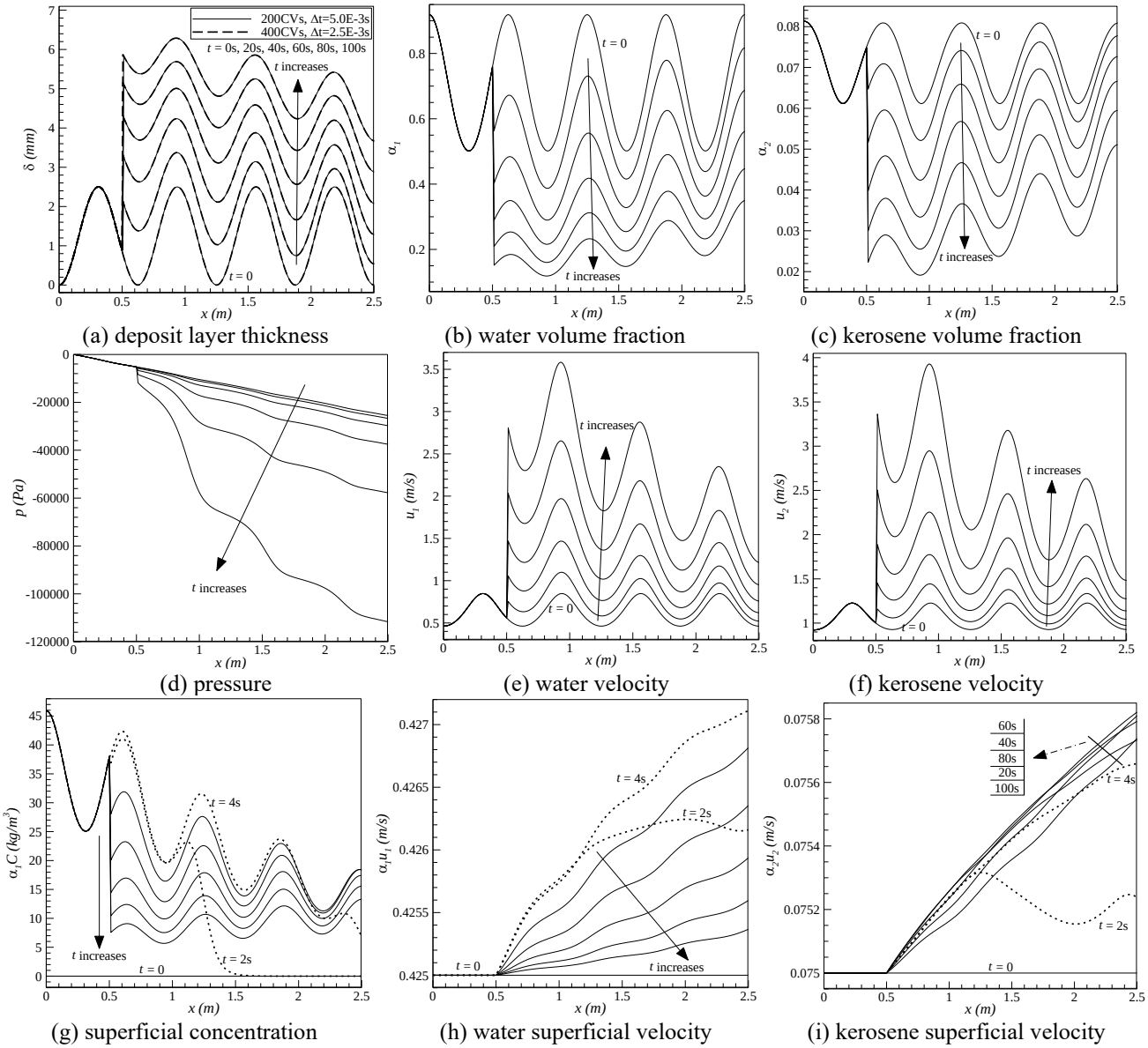

Figure 11. Deposition in a sinusoidal pipe with *l=L*/4

The solutions are shown respectively in Figure 10 and 11. Generally, the pipe geometry affects the deposition process closely. For a sinusoidal pipe with *l=L*, the pipe first converges reaching a minimum cross section at *x=L/2* then diverges downstream to a maximum cross section at *x=L*. Because of the pipe geometry, location of smallest flow area ($\alpha_1+\alpha_2$) after formation of deposit layer is no longer at *x*=0.5m where deposition starts to occur. It is shifted instead downstream to *x=L/2*. Both water and kerosene velocities first increases prior to *x=L/2* and then decreases downstream (Figures 10e and 10f) with a profile associated very closely to that of the available flow area variation (see the plot of δ in Figure 10a).

Pressure gradient is distinctly different in the range of $0 \le x < 0.5$, $0.5 \le x < 1.25$ and $1.25 \le x < 2.5$. For the range of $0 \le x < 0.5$, the pressure gradient does not change with time as no deposit is formed there. For the range of $0.5 \le x < 1.25$, even with deposit formed, the flow area decreases along pipe resulting in a increasingly larger pressure gradient. However, at *t*=100s the flow area is almost constant along the pipe, giving an almost constant pressure gradient. For the range of $1.25 \le x < 2.5$, the flow area increases along the pipe. The pressure gradient then becomes smaller than that in the range of $1.25 \le x < 2.5$.

For sinusoidal pipe with *l=L/4* (Figure 11), the pipe becomes wavy. Familiar features found in sinusoidal pipe of *l=L* are observed. The flow area varies sinusoidally along the pipe (Figure 11a) and generally increasing downstream as thinner deposit is formed downstream. This is consistent as less particles are transported downstream because of deposition. Pressure drop along the pipe responses closely to the flow area of distinct wavy features (Figure 11d).

6. CONCLUSIONS

A model is developed for particle deposition in two-phase flow in vertical pipes. There are three modules with each accounting for different physical phenomenon in this model: Fluid Transport, Particle Transport and Particle Deposition, each tightly coupled to the others. A limiting case with analytical solutions and two experimental works are employed to respectively verify and validate the capability of the model. The model is then demonstrated for deposition in two-phase flow in pipe of constant cross section. The model is also shown to be easily adaptable to pipe of varying cross section. The results demonstrate the importance of fully-coupling the three

modules.

In the current model, particles are carried into the pipe at the inlet. Comparatively, particle concentration is higher upstream. For pipes of constant cross section, the deposit layer grows very fast upstream and it is thickest at the axial location where deposition starts to occur. This is also observed in two-dimensional modeling, although the location is slightly downstream of where deposition starts to occur as particles needs to transported to the wall while simultaneously travel over finite axial distance downstream.

In addition to be carried into the pipe at the inlet, particles can actually be generated thermodynamically (or chemically) within the pipe. Then, in addition to the above three modules, a module modeling thermodynamics (or chemistry) of the particle generation process is required. An additional source term to account for particle generation is then added to Particle Transport governing equation, i.e. Eq. (8). Under this condition, location of thickest deposit layer is generally not the axial location where deposition starts to occur.

REFERENCES

[1] Bai, X., Luo, T., Cheng, K., Chai, F. (2014). Experimental Study on fouling in the heat exchangers of surface water heat pumps. Applied Thermal Engineering, 70: 892-895. https://doi.org/10.1016/j.applthermaleng.2014.06.009

[2] Rittirong, A., Panacharoensawad, E., Sarica, C. (2015). An experimental study of paraffin deposition under two-phase gas-oil slug flow in horizontal pipes. Offshore Technology Conference, Houston, Texas, USA, May 4-7. https://doi.org/10.4043/26047-MS

[3] Zheng, S. (2017). Wax deposition from single-phase oil flows and water-oil two-phase flows in oil transportation pipelines. PhD Thesis, University of Michigan, US.

[4] Polyanskiy, T.A., Zaitsev, A.V., Gulyaev, I.P., Gurin A.M. (2018). Numerical and experimental investigation of two phase flow for direct metal deposition. Journal of Physics: Conference Series (Beam Technologies and Laser Application), 1109: 012010. https://doi.org/10.1088/1742-6596/1109/1/012010

[5] Adeyanju, O.A., Oyekunle, L.O. (2019). Experimental study of water-in-oil emulsion flow on wax deposition in subsea pipelines. Journal of Petroleum Science and Engineering, 182: 106294. https://doi.org/10.1016/j.petrol.2019.106294

[6] Chi, Y., Sarica, C., Daraboina, N. (2019). Experimental investigation of two-phase gas-oil stratified flow wax deposition in pipeline. Fuel, 247: 113-125. https://doi.org/10.1016/j.fuel.2019.03.032

[7] Husain, A., Weisman, J. (1978). Applicability of the homogeneous flow model to two phase pressure drop in straight pipe and across area changes. AIChE Symposium Series, 74: 205-214.

[8] Bansal, P.K., Rupasinghe, A.S. (1998). An homogeneous model for adiabatic capillary tubes. Applied Thermal Engineering, 18: 207-219. https://doi.org/10.1016/S1359-4311(97)00016-1

[9] Clerc, S. (2000). Numerical simulation of the homogeneous equilibrium model for two-phase flows. Journal of Computational Physics, 161: 354-375. https://doi.org/10.1006/jcph.2000.6515

[10] Ouyang, L.-B., Aziz, K. (2000). A homogeneous model for gas-liquid flow in horizontal wells. Journal of Petroleum Science and Engineering, 27: 119-128. https://doi.org/10.1016/S0920-4105(00)00053-X

[11] De Lorenzo, M., Lafon, Ph., Di Matteo, M., Pelanti, M., Seynhaeve, J.M., Bartosiewicz, Y. (2017). Homogeneous two-phase flow models and accurate steam-water table look-up method for fast transient simulations. International Journal of Multiphase Flow, 95: 199-219. https://doi.org/10.1016/j.ijmultiphaseflow.2017.06.001

[12] Hurisse, O. (2017). Numerical simulations of steady and unsteady two-phase flows using a homogeneous model. Computers & Fluids, 152: 88-103. https://doi.org/10.1016/j.compfluid.2017.04.007

[13] Maher, D, Hana, A., Habib, S. (2020). New correlations for two phase flow pressure drop in homogeneous flows model. Thermal Engineering, 67: 92-105. https://doi.org/10.1134/S0040601520020032

[14] Stevanović, V., Prica, S., Maslovarić, B. (2007). Multi-fluid model predictions of gas-liquid two-phase flows in vertical tubes. FME Transactions, 35: 173-181.

[15] Shirdel, M. (2010). Development of a coupled wellbore-reservoir compositional simulator for horizontal wells. PhD Dissertation, University of Texas, Austin.

[16] Malekzadeh, R. (2012). Severe slugging in gas-liquid two-phase pipe flow. PhD Dissertation, Delft University of Technology, Netherlands.

[17] Malekzadeh, R., Belfroid, S., Mudde, R. (2012). Transient drift flux modelling of severe slugging in pipeline-riser systems. International Journal of Multiphase Flow, 46: 32-37. https://doi.org/10.1016/j.ijmultiphaseflow.2012.06.005

[18] Choi, J., Pereyra, E., Sarica, C., Lee, H., Jang, I.S., Kang, J. (2013). Development of a fast transient simulator for gas-liquid two-phase flow in pipes. Journal of Petroleum Science and Engineering, 102: 27-35. https://doi.org/10.1016/j.petrol.2013.01.006

[19] Teixeira, R.G.D., Secchi, A.R. (2017). Assessment of the accuracy and dynamic simulation capabilities of liquid-vapour two-phase flow separated and mixture models. Computer Aided Chemical Engineering, 40: 2095-2100. https://doi.org/10.1016/B978-0-444-63965-3.50351-2

[20] Zhang, J., Wu, Q.L., Liu, S., Xu, J.Y. (2020). Investigation of the gas-liquid two-phase flow and separation behaviors at inclined T-junction pipelines. ACS Omega, 5(34): 21443-21450. https://doi.org/10.1021/acsomega.0c01805

[21] Wu, J., Li, X., Liu, H., Zhao, K., Liu S. (2020). Calculation method of gas-liquid two-phase boiling heat transfer in helically-coiled tube based on separated phase flow model. International Journal of Heat and Mass Transfer, 161: 120242. https://doi.org/10.1016/j.ijheatmasstransfer.2020.120242

[22] Davis, R., Moore, E., Zachariah, M. (1993). Numerical modeling of particle dynamics in a rotating disk chemical vapor deposition reactor. Journal of Crystal Growth, 132: 513-522. https://doi.org/10.1016/0022-0248(93)90079-C

[23] Saylor, R.D., Baker, B.D., Lee, P., Tong, D., Pan, L., Hicks, B.B. (2019). The particle dry deposition component of total deposition from air quality models: right, wrong or uncertain? Tellus B: Chemical and Physical Meteorology, 71: 1-22.

https://doi.org/10.1080/16000889.2018.1550324
[24] Ge, W., Sankaran, R. (2019). An adaptive particle tracking algorithm for lagrangian-eulerian simulations of dispersed multiphase flows. 2019 AIAA SciTech Forum, San Diego, California, January 7-11.
[25] Talebizadehsardari, P., Rahimzadeh,H., Ahmadi, G., Inthavong, K., Keshtkar, M.M., Moghimi, M.A. (2020). Nano-particle deposition in laminar annular pipe flows. Advanced Powder Technology, 31: 3134-3143. https://doi.org/10.1016/j.apt.2020.06.005
[26] Van Veldhuizen, S., Vuik, C., Kleijn, C. (2007). Comparison of numerical methods for transient cvd simulations. Surface and Coatings Technology, 201: 8859-8862. https://doi.org/10.1016/j.surfcoat.2007.04.022
[27] Yuan, H., Shapiro, A.A. (2010). Modeling non-fickian transport and hyperexponential deposition for deep bed filtration. Chemical Engineering Journal, 162: 974-988. https://doi.org/10.1016/j.cej.2010.07.003
[28] Wen, S., Shin, Y.C. (2011). Modeling of transport phenomena in direct laser deposition of metal matrix composite. International Journal of Heat and Mass Transfer, 54: 5319-5326. https://doi.org/10.1016/j.ijheatmasstransfer.2011.08.011
[29] Pilou, M., Antonopoulos, V., Makris, E., Neofytou, P., Tsangaris, S., Housiadas, C. (2013). A fully Eulerian approach to particle inertial depositionin a physiologically realistic bifurcation. Applied Mathematical Modelling, 37: 5591-5605. https://doi.org/10.1016/j.apm.2012.10.055
[30] Xu, Z., Han, Z., Qu, H., (2020). Comparison between Lagrangian and Eulerian approaches for prediction of particle deposition in turbulent flows. Powder Technology, 360: 141-150. https://doi.org/10.1016/j.powtec.2019.09.084
[31] Pourhashem, H., Owen, M.P., Castro, N.D., Rostami, A.A. (2020). Eulerian modeling of aerosol transport and deposition in respiratory tract under thermodynamic equilibrium condition. Journal of Aerosol Science, 141: 105501. https://doi.org/10.1016/j.jaerosci.2019.105501
[32] Chibbaro, S., Minier, J.P. (2008). Langevin PDF simulation of particle deposition in a turbulent pipe flow. Journal of Aerosol Science, 39: 555-571. https://doi.org/10.1016/j.jaerosci.2008.03.002
[33] Ge, Q. (2012). Total concentration method for modeling of deposition. MSc Thesis, The Petroleum Institute, United Arab Emirates.
[34] Su, Y., Chen, Y., Sun, X., Yan, T., Qu, J., Duan, R. (2020). Numerical simulation on the migration and deposition of micron-sized sand particles in the helical tube section during hydrate production tests. Natural Gas Industry B, 7: 410-418. https://doi.org/10.1016/j.ngib.2019.12.006
[35] Rice, H.P., Peakall, J., Fairweather, M., Hunter, T.N. (2020). Extending estimation of the critical deposition velocity in solid–liquid pipe flow to ideal and non-ideal particles at low and intermediate solid volume fractions. Chemical Engineering Science, 211: 115308. https://doi.org/10.1016/j.ces.2019.115308
[36] Derevich, I., Zaichik, L. (1988). Particle deposition from a turbulent flow. Fluid Dynamics, 23: 722-729. https://doi.org/10.1007/BF02614149
[37] Chamra, L., Webb, R. (1994). Modeling liquid-side particulate fouling in enhanced tubes. International Journal of Heat and Mass Transfer, 37: 571-579. https://doi.org/10.1016/0017-9310(94)90129-5
[38] Eskin, D., Ratulowski, J., Akbarzadeh, K. (2011). Modeling of particle deposition in a vertical turbulent pipe flow at a reduced probability of particle sticking to the wall. Chemical Engineering Science, 66: 4561-4572. https://doi.org/10.1016/j.ces.2011.06.015
[39] Kleinhans, U., Wieland, C., Frandsen, F.J., Spliethoff, H. (2018). Ash formation and deposition in coal and biomass fired combustion systems: Progress and challenges in the field of ash particle sticking and rebound behavior. Progress in Energy and Combustion Science, 68: 65-168. https://doi.org/10.1016/j.pecs.2018.02.001
[40] Soulgani, B.S., Rashtchian, D., Tohidi, B., Jamialahmadi, M. (2009). Integrated modelling methods for asphaltene deposition in wellstring. Journal of the Japan Petroleum Institute, 52: 322-331. https://doi.org/10.1627/jpi.52.322
[41] Vargas, F.M., Creek, J.L., Chapman, W.G. (2010). On the development of an asphaltene deposition simulator. Energy & Fuels, 24: 2294-2299. https://doi.org/10.1021/ef900951n
[42] Apte, M.S., Matzain, A., Zhang, H.-Q., Volk, M., Brill, J.P., Creek, J.L. (2001). Investigation of paraffin deposition during multiphase flow in pipelines and wellbores-part 2: Modeling. Journal of Energy Resources Technology, 123: 150-157. https://doi.org/10.1115/1.1369359
[43] Xiao, J., Shonham, O., Brill, J. (1990). A comprehensive mechanistic model for two-phase flow in pipelines. SPE Annual Technical Conference and Exhibition, New Orleans, Louisiana, September 23-26. https://doi.org/10.2118/20631-MS
[44] Kaya, A.S. (1998). Comprehensive mechanistic modeling of two-phase flow in deviated wells. MSc Thesis, University of Tulsa, Netherlands.
[45] Multiphase Solutions Inc. (MSI) (1997). A thermodynamic model for predicting vapor/liquid/solid equilibria of hydrocarbon systems. submitted to WAX JIP Members.
[46] Shagapov, V.S., Musakaev, N., Khabeev, N., Bailey, S. (2004). Mathematical modelling of two-phase flow in a vertical well considering paraffin deposits and external heat exchange. International Journal of Heat and Mass Transfer, 47: 843-851. https://doi.org/10.1016/j.ijheatmasstransfer.2003.06.006
[47] Ramirez-Jaramillo, E., Lira-Galeana, C., Manero, O. (2006). Modeling asphaltene deposition in production pipelines. Energy & Fuels, 20: 1184-1196. https://doi.org/10.1021/ef050262s
[48] Kern, D., Seaton, R. (1959). A theoretical analysis of thermal surface fouling. British Chemical Engineering, 4: 258-262.
[49] Huang, Z., Senra, M., Kapoor, R., Fogler, H.S. (2011). Wax deposition modeling of oil/water stratified channel flow. AIChE Journal, 57: 841-851. https://doi.org/10.1002/aic.12307
[50] Singh, P., Venkatesan, R., Fogler, H.S., Nagarajan, N. (2000). Formation and aging of incipient thin film wax-oil gels. AIChE Journal, 46: 1059-1074. https://doi.org/10.1002/aic.690460517
[51] Haghshenasfard, M., Yeoh, G.H., Dahari, M., Hooman, K. (2015). On numerical study of calcium sulphate fouling under sub-cooled flow boiling conditions.

Applied Thermal Engineering, 81: 18-27. https://doi.org/10.1016/j.applthermaleng.2015.01.079
[52] Bohnet, M. (2003). Influence of the transport properties of the crystal/heat transfer surface interfacial on fouling behavior. Chemical Engineering & Technology, 26: 1055-1060. https://doi.org/10.1002/ceat.200301807
[53] Duan, J., Li, J., Liu, H., Gu, K., Guan, J., Xu, S., Gong, J. (2018). A model of wax deposition under oil-gas two-phase stratified flow in horizontal pipe. Oil & Gas Science and Technology - Revue d'IFPEN, 73: 80. https://doi.org/10.2516/ogst/2018076
[54] Alhosani, A., Daraboina, N. (2020). Modeling of asphaltene deposition during oil/gas flow in wellbore. Fuel, 280: 118617. https://doi.org/10.1016/j.fuel.2020.118617
[55] Guan, Q., Chai, J.C., Goharzadeh, A., Vargas, F.M., Biswal, S.L., Chapman, W.G., Zhang, M., Yap, Y.F. (2018). A unidirectional one-dimensional approach for asphaltene deposition in large length-to-diameter ratios scenarios. Journal of Petroleum Science and Engineering, 166: 857-870. https://doi.org/10.1016/j.petrol.2018.03.056
[56] Ishii, M., Mishima, K. (1984). Two-fluid model and hydrodynamic constitutive relations. Nuclear Engineering and Design, 82: 107-126. https://doi.org/10.1016/0029-5493(84)90207-3
[57] Xu, J., Wong, T.N., Huang, X. (2006). Two-fluid modeling for low-pressure subcooled flow boiling, International Journal of Heat and Mass Transfer, 49: 377-386. https://doi.org/10.1016/j.ijheatmasstransfer.2004.12.051
[58] Guan, Q., Goharzadeh, A., Chai, J.C., Vargas, F.M., Biswal, S.L., Chapman, W.G., Zhang, M., Yap, Y.F. (2018). An Integrated Model for Asphaltene Deposition in Wellbores/Pipelines above Bubble Pressures. Journal of Petroleum Science and Engineering, 169: 353-373. https://doi.org/10.1016/j.petrol.2018.05.042
[59] Maqbool, T., Raha, S., Hoepfner, M.P., Fogler, H.S. (2011). Modeling the Aggregation of Asphaltene Nanoaggregates in Crude Oil−Precipitant Systems. Energy Fuels, 25: 1585-1596. https://doi.org/10.1021/ef1014132
[60] Stosic Z., Stevanovic, V. (2001). Prediction methods for interfacial drag in transitional two-phase flow regimes. Proceedings of the 5th World Conference on Experimental Heat Transfer, Fluid Mechanics and Thermodynamics, September 24-28, Thessaloniki, Greece.
[61] Richter, H. (1983). Separated two-phase flow model: Application to critical two-phase flow. International Journal of Multiphase Flow, 9: 511-530. https://doi.org/10.1016/0301-9322(83)90015-0
[62] Patankar, S.V. (1980). Numerical Heat Transfer and Fluid Flow, Hemisphere Publisher.
[63] Darwish, M., Moukalled, F., Sekar, B. (2001). A unified formulation of the segregated class of algorithms for multifluid flow at all speeds. Numerical Heat Transfer: Part B: Fundamentals, 40: 99-137. ttps://doi.org/10.1080/104077901750475887
[64] Li, X. (2016). Modeling of Two-phase Flow with Deposition in Vertical Pipes. M.Sc. Thesis, Petroleum Institute, Abu Dhabi, UAE.
[65] Suguimoto, F.K., Mazza, R.A. (2015). Experimental analysis of pressure gradients on a liquid-liquid two phase flow, IV Journeys in Multiphase Flows (JEM 2015), March 23-27, Campinas, SP, Brazil.
[66] Rodriguez, O., Bannwart, A., De Carvalho, C. (2009). Pressure loss in core-annular flow: Modeling, experimental investigation and full-scale experiments, Journal of Petroleum Science and Engineering, 65: 67-75. https://doi.org/10.1016/j.petrol.2008.12.026

NOMENCLATURE

A	cross-sectional area, m^2
a_{wk}	interfacial area concentrations, m^{-2}
C	particle concentration, kg/m^3
C'	virtual mass coefficient, -
C_{FI}	interfacial friction factor, -
C_D	drag coefficient for a single bubble, -
D	pipe diameter, m
D_B	bubble diameter, m
$D_{B,\max}$	bubble maximum diameter, m
D_h	hydraulic diameter, m
F_{wk}	wall shear forces, N
F_{12}	interfacial drag force, N
f_{wk}	friction coefficient, -
J	superficial velocity, m/s
g	gravitational acceleration, m/s^2
k	deposition rate constant, s^{-1}
$\dot{M}_D$	deposition generation rate, $kg/(m^3 \cdot s)$
m	reaction order for deposition, -
p	pressure, Pa
Re_k	Reynolds number, -
Re_B	bubble Reynolds number, -
S	wetted diameter, m
S_φ	source term, -
t	time, s
u	fluid velocity, m/s
$\vec{u}$	velocity vector, -
V	volume, m^3
x	axial location along the flow direction, m

Greek symbols

α	volume fraction, m^3/m^3
α'	relative volume fraction, m^3/m^3
δ	deposit thickness, mm
μ	dynamic viscosity, Pa·s
ρ	density, kg/m^3
$\tilde{\rho}$	appropriate ‘density’, -
τ	shear stress, N/m^2
σ	surface tension, N/m
φ	variable of interest, -

Subscripts

A	annular flow
B	bubbly flow
$B\text{-}T$	bubbly flow to transitional flow

d	deposit
i	flow cross section
k	fluid 1 or 2
m	mixture
r	relative
T-A	transitional flow to annular flow
w	water
1	fluid 1
2	fluid 2

APPENDIX: CALCULATION OF INTERFACIAL FORCES

Interfacial Forces between the Wall and Fluid *k*

The interfacial forces between the wall and fluid *k* are given by [60] as:

$$F_{wk} = a_{wk}\tau_{wk}, \quad k = 1,2 \tag{A-1}$$

where, the wall shear stress τ_{wk} can be calculated as

$$\tau_{wk} = f_{wk}\frac{\rho_k |u_k| u_k}{2} \tag{A-2}$$

In the above equation, the friction coefficient f_{wk} is determined as:

$$f_{wk} = \begin{cases} 16\,\mathrm{Re}_k^{-1}, & \text{laminar flow} \\ 0.079\,\mathrm{Re}_k^{-0.25}, & \text{turbulent flow} \end{cases} \tag{A-3}$$

Both interfacial area concentration a_{wk} and Reynolds numbers Re_k are flow pattern specific. Only three flow patterns are considered: bubbly, transitional and annular flows. These flow patterns are demarcated using the fluid 2 relative volume fraction α_2' as:

$$\begin{cases} \alpha_2' \le \alpha_{B-T}' & \text{, bubly} \\ \alpha_{B-T}' < \alpha_2' < \alpha_{T-A}' & \text{, transitional} \\ \alpha_2' \ge \alpha_{T-A}' & \text{, annular} \end{cases} \tag{A-4}$$

where,

$$\alpha_k' = \frac{\alpha_k}{\alpha_1 + \alpha_2}, \quad k = 1,2 \tag{A-5}$$

The relative volume fraction for the transition from bubbly to transitional flow is set to $\alpha_{B-T}' = 0.25$. For the transition of transitional to annular flow, $\alpha_{T-A}' = 0.80$. Note the subscripts B, T and A for respectively bubbly, transitional and annular flows.

For bubbly flow,

$$a_{wk} = \frac{4\alpha_k'}{D_h} \tag{A-6a}$$

$$\mathrm{Re}_k = \frac{\rho_k u_k D_h}{\mu_k} \tag{A-6b}$$

where, hydraulic diameter D_h is given by

$$D_h = \frac{4A}{S} \tag{A-6c}$$

The flow area A and wetted diameter S are given respectively by:

$$A = (1-\alpha_d)\frac{\pi D^2}{4} \tag{A-6d}$$

$$S = (1-\alpha_d)^{0.5}\pi D \tag{A-6e}$$

where, the pipe diameter D.

For annular flow, the wall shear force F_{w2} is negligible [61]. For fluid 1:

$$a_{w1} = \frac{S_{w1}}{A} \tag{A-7a}$$

$$\mathrm{Re}_1 = \frac{\rho_1 u_1 D_{h1}}{\mu_1} \tag{A-7b}$$

where, hydraulic diameters D_{h1} is defined by:

$$D_{h1} = \frac{4A_1}{S_{w1}} \tag{A-7c}$$

The flow area A_1 and perimeter of fluid 1-wall interface S_{w1} are given respectively by:

$$A_1 = \alpha_1' A \tag{A-7d}$$

$$S_{w1} = \pi D_h \tag{A-7e}$$

For transitional flow, interfacial area concentrations and shear stresses are interpolated respectively as:

$$Z = K_1^3 Z_B + K_2^{1/3} Z_A \tag{A-8a}$$

$$K_1 = \frac{\alpha_{T-A}' - \alpha_2'}{\alpha_{T-A}' - \alpha_{B-T}'}, \quad K_2 = \frac{\alpha_2' - \alpha_{B-T}'}{\alpha_{T-A}' - \alpha_{B-T}'} \tag{A-8b}$$

$$Z_i \in \{a_{wk,i}, \tau_{wk,i}\}, \quad i = B, A \tag{A-8c}$$

Interfacial Drag Force F_{12}

The interfacial drag force between the two fluids F_{12} is modeled as [57]:

$$F_{12} = \frac{2C_{FI}}{D_h}\sqrt{\alpha_2'}\rho_2(u_2-u_1)|u_2-u_1| + C'\alpha_2'\rho_1 u_2 \frac{d(u_2-u_1)}{dx} \tag{A-9}$$

where, the virtual mass coefficient C' is given by:

$$C' = \begin{cases} 0.5, & \text{bubbly flow} \\ 0 & , \text{ other} \end{cases} \tag{A-10}$$

The interfacial friction factor C_{FI} for bubbly and annular flows is given by:

$$C_{FI} = \begin{cases} C_D\sqrt{\alpha_2'}(1-\alpha_2')^{-1.7}\dfrac{\rho_1}{\rho_2}\dfrac{D_h}{D_B}, & \text{bubbly flow} \\ 0.005[1+75(1-\alpha_2')] & , \text{ annular flow} \end{cases} \tag{A-11a}$$

Note that for bubbly flow, the drag coefficient for a single bubble C_D is defined as:

$$C_D = \begin{cases} \dfrac{24}{\mathrm{Re}_B}(1+0.15\,\mathrm{Re}_B^{0.687}), & \mathrm{Re}_B < 1000 \\ 0.44 & , \ \mathrm{Re}_B \geq 1000 \end{cases} \tag{A-11b}$$

with,

$$\mathrm{Re}_B = \frac{\rho_1 D_B(1-\alpha_2')|u_2-u_1|}{\mu_1} \tag{A-11c}$$

$$D_B = 0.0615\,D_{B,\max} \tag{A-11d}$$

$$D_{B,\max} = 3168\,D_h^{2/5}\left(\frac{\sigma}{\rho_1}\right)^{3/5}\left(\frac{\rho_1}{\rho_2}\right)^{1/5}u_m^{6/5} \tag{A-11e}$$

$$u_m = (\alpha_1'\rho_1 u_1 + \alpha_2'\rho_2 u_2)/\rho_m \tag{A-11f}$$

$$\rho_m = \alpha_1'\rho_1 + \alpha_2'\rho_2 \tag{A-11g}$$

where, Re_B, D_B, $D_{B,max}$, u_m and ρ_m are respectively bubble Reynolds number, mean gas bubble diameter, bubble maximum diameter, averaged two-phase flow velocity and two-phase mixture density.

For transitional flow, C_{FI} is the interpolated linearly as:

$$C_{FI} = C_{FI,B} + \frac{C_{FI,B}-C_{FI,A}}{\alpha_{B-T}'-\alpha_{T-A}'}(\alpha_2'-\alpha_{B-T}') \tag{A-11h}$$